Journal of Nuclear Materials 385 (2009) 504–509

Contents lists available at ScienceDirect

Journal of Nuclear Materials

journal homepage: www.elsevier.com/locate/jnucmat

Compatibility of martensitic/austenitic steel welds with liquid lead bismuth eutectic environment

J. Van den Bosch *, A. Almazouzi

SCK●CEN (Belgian Nuclear Research Centre), Boeretang 200, B-2400 Mol, Belgium

ARTICLE INFO

Article history:
Received 2 October 2008
Accepted 5 December 2008

PACS:
61.25.Mv
61.82.Bg
62.20.Mk
68.03.Cd
68.08.−p
81.20.Vj

ABSTRACT

The high-chromium ferritic/martensitic steel T91 and the austenitic stainless steel 316L are to be used in contact with liquid lead–bismuth eutectic (LBE), under high irradiation doses. Both tungsten inert gas (TIG) and electron beam (EB) T91/316L welds have been examined by means of metallography, scanning electron microscopy (SEM-EDX), Vickers hardness measurements and tensile testing both in inert gas and in LBE. Although the T91/316L TIG weld has very good mechanical properties when tested in air, its properties decline sharply when tested in LBE. This degradation in mechanical properties is attributed to the liquid metal embrittlement of the 309 buttering used in TIG welding of T91/316L welds. In contrast to mixed T91/316L TIG welding, the mixed T91/316L EB weld was performed without buttering. The mechanical behaviour of the T91/316L EB weld was very good in air after post weld heat treatment but deteriorated when tested in LBE.

1. Introduction

In modern society, the welding procedure is one of the most important – if not the most-connection techniques available. An incredibly wide variety of utensils and structures from the most simple such as a spoon to the most complicated like off-shore platforms, ships or even nuclear reactors could only be realised by application of one or several welds.

One nuclear reactor type that has received a lot of attention lately is the accelerator driven system (ADS) [1,2]. It is proposed as one of the possible solutions to reduce the high level radio-active waste and burn up the long lived actinides resulting from the fission reactors. The ADS technology however, requires severe operating conditions. The structural materials and their weldments need to withstand temperatures ranging between 473 and 823 K under high neutron flux and in contact with liquid metal.

Within the EUROTRANS Demetra project the ferritic/martensitic steel T91 and the austenitic stainless steel 316L have been chosen as the main candidate structural materials for the construction of the ADS under study. These high chromium steels will need to be welded (both similar and dissimilar welds) successfully and their weldments will undergo stringent conditions similar to the environmental conditions of the base materials. The possible susceptibility to liquid metal embrittlement (LME) of these welds could be a critical issue and therefore needs to be examined.

When welding, the welded structure needs to have the same or comparable mechanical and corrosion properties in the weld and the heat affected zone (HAZ) than in the base metal. It is e.g., unacceptable that the weld would have lower toughness or that the ductile-to-brittle transition temperature shift is significantly higher in the weld than in the base materials. For the corrosion resistance of the structure it can also not be acceptable that the corrosion resistance of austenitic stainless steels would be lost in the HAZ due to sensitisation.

Although welding high chromium steels has become a well known technique, the performance of high Cr and Cr–Mo steel weldment is still considered to be a life limiting factor at high temperatures. In fact, a high percentage of failures in the power industry have been reported to be welding related [3].

Within the Spire project and in the frame of MEGAPIE the importance of examining welds of T91 and 316L(N) was recognised and some irradiations were performed in SINQ [4,5] as well as in contact with LBE [6]. The fast breeder and fusion community have also produced interesting results on welds which can be very useful for the ADS community such as the investigation of EB and TIG welded EM10 to relatively high doses [7] and the re-weldability studies on 316L(N) [8].

In this paper, we will firstly present the technical information on the welding process of the examined welds as well as the applied post weld heat treatment (PWHT). Afterwards the microstructure and mechanical behaviours of both the T91/316L TIG and EB welds will be described in detail.

* Corresponding author. Tel.: +32 14 33 31 77; fax: +32 14 32 12 16.
E-mail address: jvdbosch@sckcen.be (J. Van den Bosch).

0022-3115/$ - see front matter © 2008 Elsevier B.V. All rights reserved.
doi:10.1016/j.jnucmat.2008.12.043

2. Experimental

The composition of both the T91 and 316L steels as well as the composition of the buttering material and the weld deposit material for the TIG weld are given in Table 1.

The T91/316L weld was performed in two phases by CMI, Belgium. At first a high alloyed 309 alloy was welded by SAW onto the T91 in five passes using an Arosta 309S electrode of Ø 2.5–3.2 mm while the T91 steel was preheated to a minimal temperature of 523 K. This procedure is called beurrage or buttering.

Table 1
Chemical composition of the T91 and 316L base materials as well as the buttering material (309) and the weld deposit material (Nertalinox), wt%.

Material	B	C	N	Si	P	S	V	Cr	Mn	Ni	Nb	Mo
T91	<1 wppm	0.1	0.04	0.22	0.021	0.0004	0.21	8.99	0.38	0.11	0.06	0.89
316L	<1 wppm	0.019	0.03	0.67	0.032	0.0035	0.07	16.7	1.81	9.97	–	2.05
309	–	0.02	–	0.82	0.02	0.018	–	23.3	0.8	12.5	–	0.08
Nertalinox	–	0.012	–	0.34	0.014	0.004	–	18.64	1.51	11.61	–	2.57

Table 2
Thermodynamic and mechanical data of T91 and 316L.

Material	Melting temperature (K)	Thermal conductivity[a] ($W\,m^{-1}K^{-1}$)	Thermal expansion coefficient[a] ($10^{-6}\,K^{-1}$)	Specific heat ($J\,kg^{-1}\,K^{-1}$)	Latent Heat of fusion ($J\,kg^{-1}$)	Yield strength[a] ($\sigma_{0.2}$) (MPa)	Tensile strength[a] (σ_{UTS}) (MPa)	Total elongation[a] (ε_{tot}) (%)	Uniform elongation[a] (ε_{unif}) (%)
T91	1773	22.1	10.4	444.8	2.6×10^5	580	708	21	6.6
316L	1648	13.49	15.2	500	3.3×10^5	308	639	84	12

[a] At room temperature.

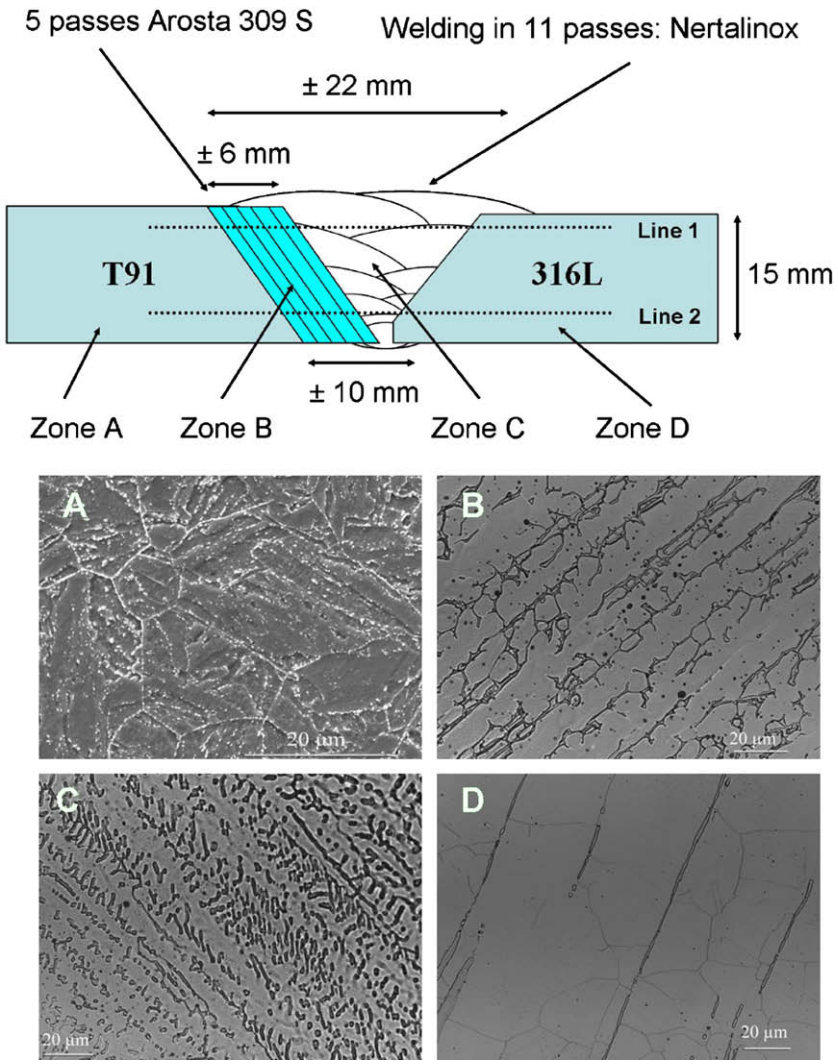

Fig. 1. Schematic representation and microstructure of the 316L/T91 TIG weld joint. Zone A: Martensitic T91 steel base material; zone B: 309 steel buttering; zone C: TIG weld deposit (Nertalinox); zone D: Austenitic 316L stainless steel base material with δ-ferrite. Line 1 and 2 indicate the location of the Vickers hardness measurements across the T91/316L TIG weld (see Fig. 4).

Commercially, two options are used standard for mixed welding of austenitic 300 grade type steel to ferritic and martensitic steels. Either the buttering is done using an Inconel alloy, or performed using over alloyed 309. For application in ADS or other LBE cooled systems, the Inconel option cannot be used since Ni is highly soluble in LBE. Therefore, the buttering of the TIG weld under investigation was done using 309 alloy.

After buttering, a PWHT was performed in order to relieve stresses by heating up the plate starting from room temperature at a maximum heating rate of 100 K h^{-1} up to 1013 K and holding it for 45 min. Cooling was performed at a controlled rate of maximum 95 K h^{-1} down to 323 K when the plate was removed from the furnace.

In a second phase, the actual connection weld was made between the 316L plate and the over alloyed 309 side of the T91 plate. This weld comprised of 11 passes in total. The thermodynamic parameters of both T91 and 316L, relevant to the welding process are summarised in Table 2.

The T91/316L TIG weld, schematically represented in Fig. 1, consists of four zones: the base materials: T91 and 316L steels, the filler material in 316L alloy (NERTALINOX) and the buttering material, being 309 alloy.

The T91/316L electron beam weld was performed by FZK, Germany using an EBW 1001/10-60 CNC from PTR Präzisiontechnik, Maintal, Germany. The welding machine has a maximum voltage of 60 kV and a maximum current of 167 mA. The vacuum chamber has a dimension of 580 mm by 350 mm with a height of 500 mm. Prior to welding, the parts to be welded were degreased and fixed together by one single pass of TIG welding. When placed in the vacuum chamber, the chamber was pumped down to about 6×10^{-5} Pa. Applied electrical tension during EB welding for the weldments under investigation was 60 kV, at a current of 62 A. The welding travel speed was 10 mm s^{-1}. The weldments were made available in the as welded condition.

Both welded joints were mechanically polished to a 1 μm fine grain in order to analyze their microstructure. The TIG weld was first etched using Villela's reagent to reveal the microstructure of the T91 steel (zone A in Fig. 1), and then electro-polished (97% acetic acid, 3% perchloric acid) to reveal the microstructure of the austenitic steels (zones B, C and D in Fig. 1). The sample was observed using optical microscopy and scanning electron microscopy (SEM). The micrographs of the different zones of the 316L/T91 TIG weld joint are depicted in Fig. 1 below the schematic representation of the TIG weld.

The microstructure of the T91 steel (zone A) consists of a tempered martensite (Fig. 1A). The microstructure of the 309 filler material (zone B) is dendritic (Fig. 1B) as well as this of the 316L filler alloy (Nertalinox), with dendrite morphology depending on the pass number (Fig. 1C). The microstructure of the 316L base material consists of austenite grains and delta ferrite islands (Fig. 1D) which were confirmed by X-ray diffraction. The presence of delta ferrite is related to the composition of the steel, especially its relatively low nickel content. No porosity or micro-crack was observed at the interface between the different zones.

The T91/316L EB weld was etched using Villela's reagent to visualise its T91 side and later etched using a solution of 100 ml HCl, 33 ml HNO_3 and a few drops of H_2SO_4 to reveal the austenitic microstructure of the 316L side. Despite the higher melting point of T91 compared to this of 316L as mentioned in Table 2, the higher heat conductivity and lower latent heat of fusion of the ferritic/martensitic T91 caused more T91 to be melted and added into the weld than 316L. Therefore, the area that was molten has a martensitic microstructure as depicted in Fig. 2.

Fig. 2 also shows the chemical profile across the electron beam weld. It can be seen that the changes in composition are very sharp. This is expected to change after ageing due to long term exposure of the welded connection at elevated temperatures and may lead to sensitisation of the T91/316L EB weld. This is however outside the scope of this work.

To perform tensile tests, cylindrical small size tensile samples were machined with a gauge length of 12 mm, a diameter of 2.4 mm and a total length of 24 mm. Due to the complex nature of the T91/316L TIG weld, the samples were taken in different orientations along the weld. Samples were taken across the weld with either the HAZ on the T91 side or the HAZ on the 316L side in the middle of the gauge and inside the 316L weld material.

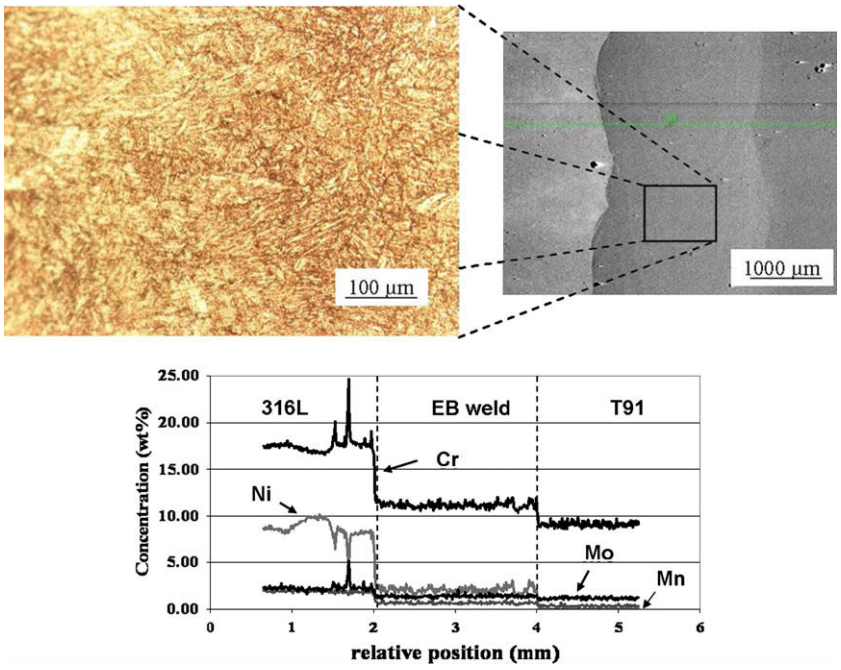

Fig. 2. Martensitic microstructure of the weldment and chemical composition (Cr, Mn, Ni, and Mo) across the T91/316L EB welded joint as measured by EDX.

The T91/316L EB weld however, was sufficiently narrow to machine samples across the weld, having the area that had been molten in the middle of the gauge.

3. Results and discussion

3.1. T91/316L TIG weld

We performed hardness tests at room temperature across the weld on the upper side of the weld (line 1 in Fig. 1), as well as on the lower part (line 2 in Fig. 1) to verify the quality of the weld. The Vickers hardness values corresponding with line 1 are on the left axis, while those corresponding with line 2 are on the right axis. This allowed distinction of the four zones of the TIG weld in both hardness profiles. In Fig. 3, the T91 base metal is located on the left side of the profile. The hardness profile shows a significant increase on the T91 side and reaches a maximum at the interface with the 309 buttering alloy. This is typical for mixed welds of martensitic steels to austenitic steels. The PWHT is actually too short to relieve all stresses from welding on the T91 side, but the PWHT softens the 316L side with increasing duration of PWHT. Therefore, the holding time of 45 min is considered to be the optimum compromise for a weld of 15 mm thickness.

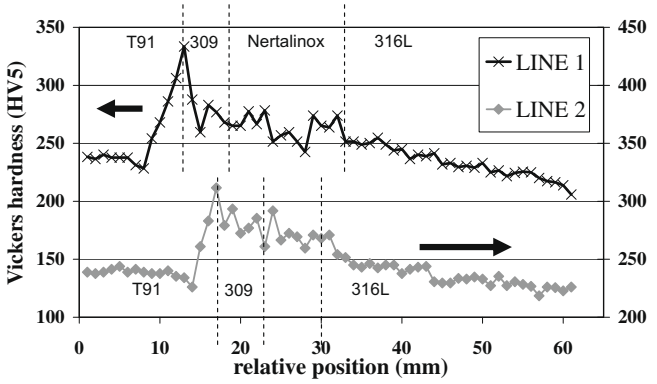

Fig. 3. Vickers hardness measurement across the T91/316L TIG weld along Line 1 and 2 indicated in the schematic representation of the T91/316L TIG weld in Fig. 1. Vickers hardness of Line 1 indicated on the left scale. Vickers hardness of Line 2 indicated on the right scale.

Tensile tests were performed at 623 K in three different orientations at a strain rate of $5 \times 10^{-6}\,s^{-1}$. The stress–strain curves are depicted in Fig. 4, along with a schematic representation of the orientation of the sample. Tests were performed both in a gas mixture of argon and 5% hydrogen and in liquid LBE. The samples tested in LBE were pre-exposed in LBE with low oxygen concentration, following the thermal cycling pattern identical to the samples in the Twin Astir irradiation experiment [9]. This thermal cycling means six periods of approximately one month each at about 630 K separated by periods of about one month at room temperature.

As shown in Fig. 4, the sample with the HAZ on the 316L side in the middle of the gauge did not undergo any liquid metal embrittlement. The sample inside the 316L weld deposit did however suffer from liquid metal embrittlement since its total elongation is significantly reduced. This effect is comparable with the embrittlement found in ferritic/martensitic steels after exposure in lead alloys with low oxygen contents [10,11] and does not represent a dramatic problem since sufficient ductility is still present. The sample with the HAZ on the T91 side in the middle of the gauge however, broke in a very brittle manner displaying very little elongation and no necking at all.

It can be seen from the fracture surface of the broken sample in Fig. 5 that LME occurred at several sites indicated by arrows. The chemical mapping in Fig. 5 shows that the specimen broke in a brittle manner at the interface between the T91 and the 309 steel. The crack path partly goes through the 309 buttering in a ductile manner, however the brittle fracture is at the interface of the T91 base material with the 309 buttering. This severity of liquid metal embrittlement is probably due to the increased hardness at this location of the weld as was depicted in Fig. 3. Increased hardness of the T91 base material obtained by reducing the tempering temperature is known to increase the susceptibility of T91 steel to LME [12–14].

3.2. T91/316L EB weld

The EB weld was given a PWHT of 1013 K for 45 min with a maximum heating and cooling rate of 10 K h^{-1}. This led to a significant hardness decrease in the weld without lowering the hardness

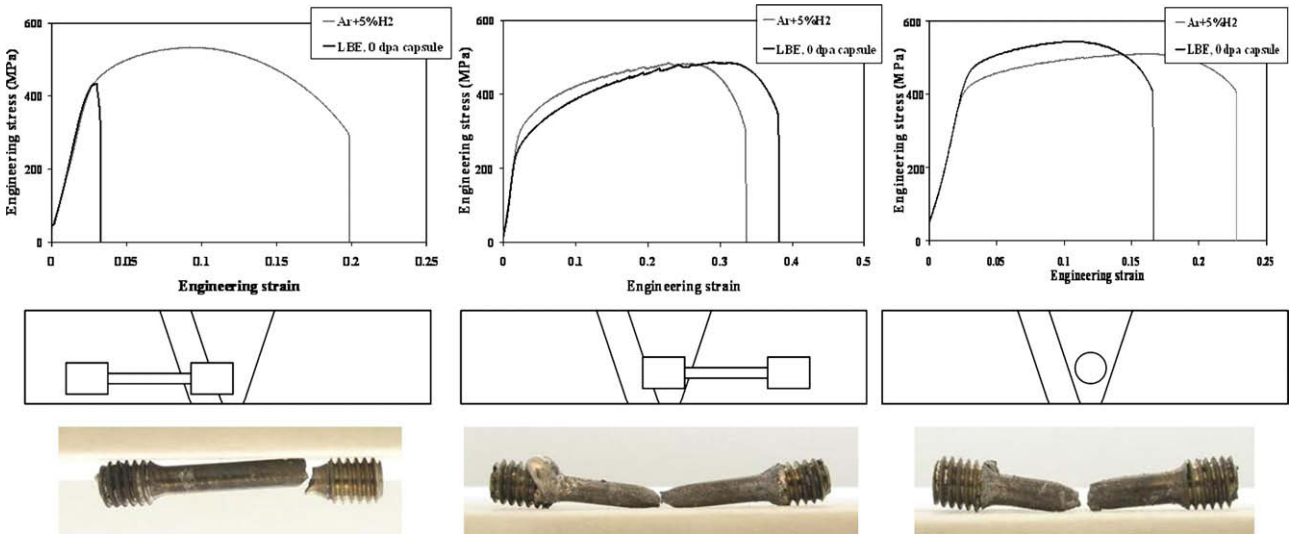

Fig. 4. Tensile results of T91/316L TIG weld tested in Ar + 5% H_2 and LBE. Schematic representation of sample orientation indicated below the stress–strain curves. Picture of the broken sample after testing in LBE depicted below the schematic representation of sample orientation.

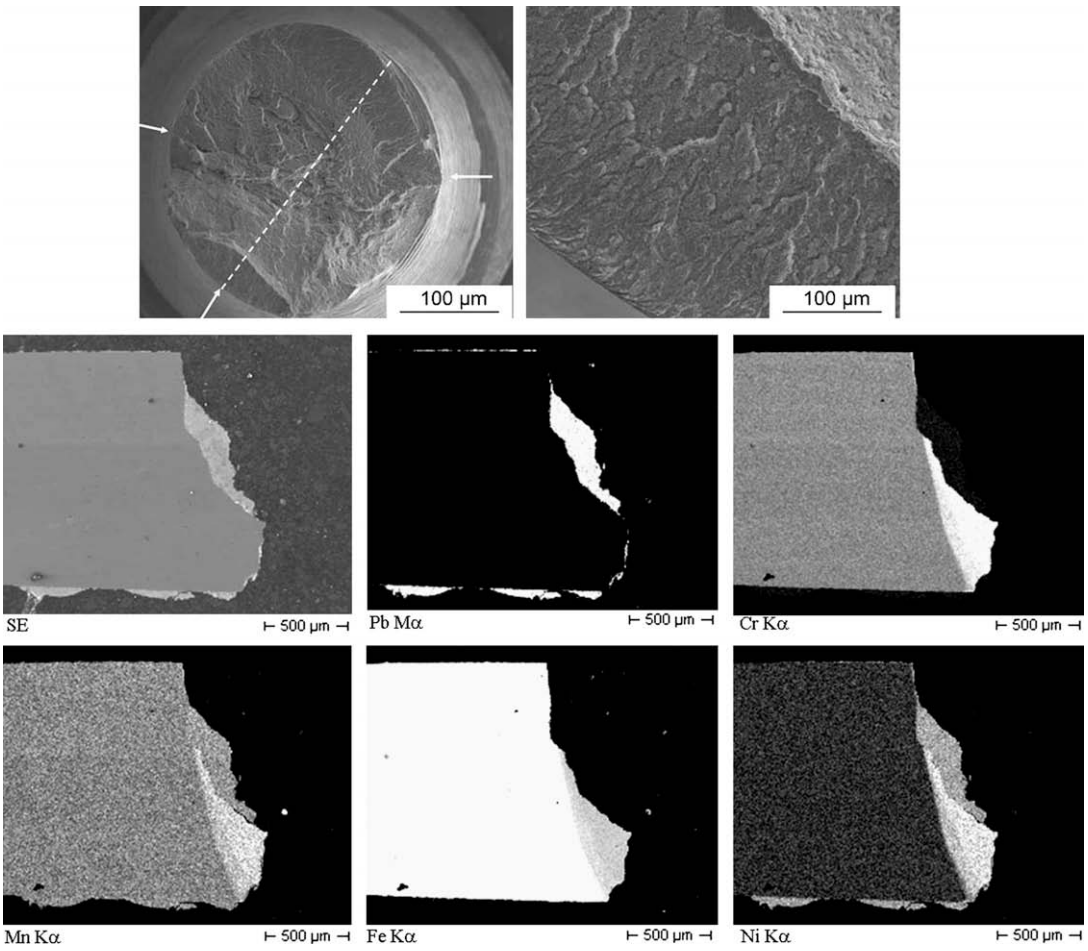

Fig. 5. Fracture surface of T91/316L TIG weld tested in LBE (shown on the left in Fig. 4) and chemical mapping of a transverse section of the broken tensile specimen. Arrows indicate the sites of LME. The dashed line in the fracture surface shows where the transverse section was taken from the other half of the broken tensile specimen.

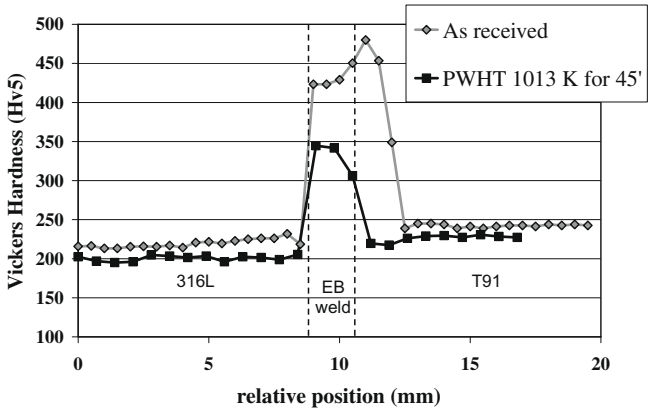

Fig. 6. Vickers hardness measurement across the T91/316L EB weld both in the as welded condition and after PWHT at 1013 K for 45 min.

of the 316L too much. The hardness profile of both the as welded and the PWHT treated EB weld are shown in Fig. 6. The hardness peak became narrower as a result of the PWHT and decreased by about 120 Hv. Furthermore, the hardness peak on the T91 steel side is strongly reduced. Despite this large hardness decrease, the hardness of the weld itself is still about 100 Hv above that of the T91 base material after PWHT. As mentioned for the T91/316L TIG weld, the applied PWHT is a compromise between softening the 316L and decreasing the welding stresses.

The tensile specimens could be taken across the weld due to the very narrow weld seam. Because we only needed to test one orientation, it allowed us to perform two tests per condition. The results of the tensile tests are depicted in Fig. 7. It can be seen that the shape of the stress–strain curve of the T91/316L EB weld is similar to that of 316L but has much less elongation. This was to be expected since the yield and tensile strength of 316L are lower than that of T91 steel. Tests in Ar + 5% H_2 show good mechanical properties. When the EB weld is tested in LBE without pre-exposure however, the specimen was broken in the weld without any necking. The fracture surface has aspects of both brittle and ductile behaviour. As depicted in the SEM picture on the lower right in Fig. 7, some initiation sites of liquid metal embrittlement can clearly be distinguished. After thermal cycling in the 0 dpa capsule of Twin Astir [9], the embrittlement is much worse and the sample breaks in the weld after very little plastic deformation. The fracture surface is predominantly brittle. Again here, the increased susceptibility to LME in the weld is attributed to the locally increased hardness of the weld.

Despite the fact that the hardness measurements presented in Fig. 3 for the TIG weld and in Fig. 6 for the EB weld were performed prior to the exposure to low oxygen containing LBE under cycling thermal conditions, the Vickers hardness values are considered to be still valid for the exposed material. The exposure in LBE was to a maximum of 630 K which is well below the M_s temperature of the T91 steel. At these temperatures, none of the alloying elements have significant mobility in the material to cause any changes in the microstructure, even after six months of exposure.

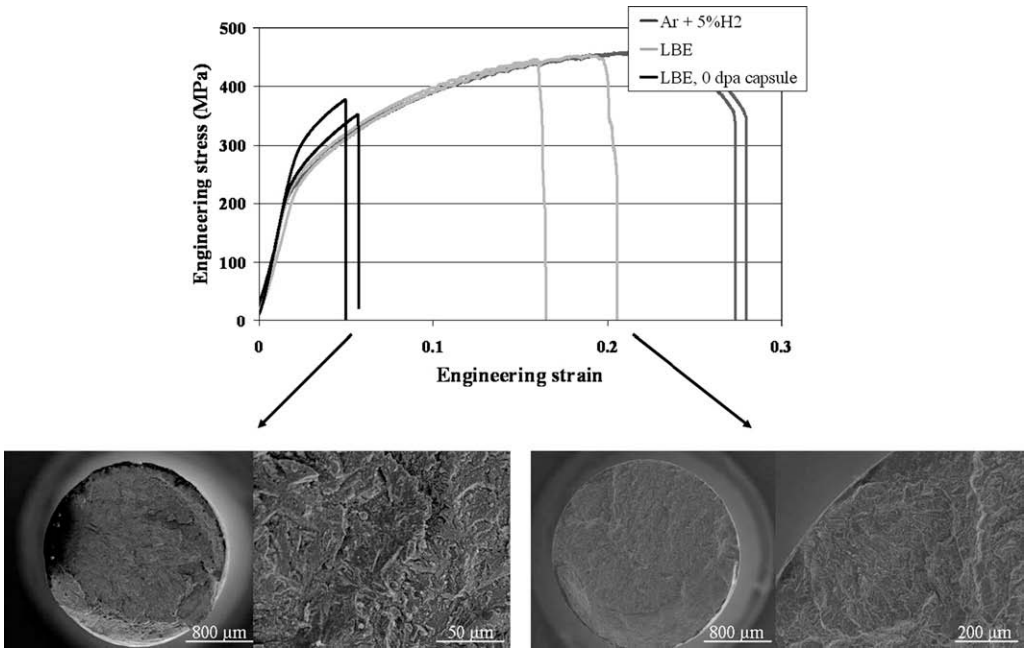

Fig. 7. Tensile results of T91/316L EB weld tested in Ar + 5%H_2 and LBE without pre-exposure and after thermal cycling in low oxygen LBE in 0 dpa capsule of Twin Astir [9]. SEM fracture surface images show mixed fracture surface when tested in LBE without pre-exposure and fully brittle fracture after thermal cycling in low oxygen LBE.

Furthermore, due to the PWHT at 1013 K for 45 min, the glissile dislocations still present in the microstructure will have minimal tendency to allow stress relaxation during exposure at 630 K. Therefore, the thermal ageing effect of the exposure is expected to be negligible and the results after exposure can be directly compared to those after PWHT. The pre-exposure to LBE under low oxygen concentration conditions is however considered to be beneficial to the wetting by the LBE.

4. Conclusions

In this paper, the microstructure of both the T91/316L TIG an EB welds was examined and their mechanical behaviour was examined in Ar + 5% H_2 and in LBE.

For the T91/316L TIG weld, buttering is needed before the two different materials can be welded together. The option of using Ni based alloys can not be used for ADS applications since Ni is highly soluble in LBE. The only industrially available alternative for TIG welding is to use 309 alloy for buttering. It is however shown here that the interface of the 309 alloy to the T91 steel is severely embrittled after thermal cycling in contact with LBE and therefore the 309 buttering technique should also not be used for LBE cooled applications.

T91/316L EB welds do not have buttering and the T91 is directly fused onto the 316L. This leads to very sudden changes in the chemical composition across the weld. Furthermore, it is shown that the T91/316L EB weld is embrittled by LBE and that the embrittlement is worse after thermal cycling in contact with LBE. The increased susceptibility to LME on the T91 side of the weld for the TIG weld and inside the weld for the EB weld is attributed to the elevated hardness in these parts of the respective welds.

Acknowledgements

The authors would like to thank I. Serre and J.-B. Vogt from the Laboratoire de Métallurgie Physique et Génie des Matériaux, Lille, France for the interesting discussions on the microstructure and mechanical properties of the T91/316L welds. Special thanks to I. Serre for performing the optical micrographs of the T91/316L TIG weld. This work was performed in the frame of the EUROTRANS-DEMETRA project (contract number FI6W-CT-2004-516520).

References

[1] L. Cinotti, B. Giraud, H. A Abderrahim, J. Nucl. Mater. 335 (2004) 148–155.
[2] H. A Abderrahim, P. Kupschus, E. Malambu, Ph. Benoit, K. Van Tichelen, B. Arien, F. Vermeersch, P. D'hondt, Y. Jongen, S. Ternier, D. Vandeplassche, Nucl. Instrum. and Meth. 463 (2001) 487.
[3] Baldev Raj, B.K. Choudhary, R.K. Singh Raman, Int. Press. Vess. Piping 81 (2004) 521.
[4] X. Jia, Y. Dai, J. Nucl. Mater. 343 (2005) 212.
[5] D. Hamaguchi, Y. Dai, J. Nucl. Mater. 343 (2005) 262.
[6] H. Glasbrenner, Y. Dai, F. Gröschel, J. Nucl. Mater. 343 (2005) 267.
[7] A. Alamo, J.L. Séran, O. Rabouille, J.C. Brachet, A. Maillard, H. Touron, J. Royer, in: Effects of Radiation on Materials: 17th International Symposium, ASTM STP 1270, 1996, pp. 761.
[8] H. Yamada, H. Kawamura, K. Tsuchiya, G. Kalinin, W. Kohno, Y. Morishima, J. Nucl. Mater. 307–311 (2002) 1584.
[9] J. Van den Bosch, A. Al Mazouzi, Ph. Benoit, R.W. Bosch, W. Claes, B. Smolders, P. Schuurmans, H. A Abderrahim, J. Nucl. Mater. 377 (2008) 206.
[10] J. Van den Bosch, D. Sapundjiev, A. Almazouzi, J. Nucl. Mater. 356 (2006) 237.
[11] J. Van den Bosch, R.W. Bosch, D. Sapundjiev, A. Almazouzi, J. Nucl. Mater. 376 (3) (2008) 322.
[12] B. Long, Z. Tong, F. Groschel, Y. Dai, J. Nucl. Mater. 377 (2008) 219.
[13] A. Legris, G. Nicaise, J.-B. Vogt, J. Foct, D. Gorse, D. Vançon, Scr. Mater. 43 (11) (2000) 997.
[14] T. Sample, H. Kolbe, J. Nucl. Mater. 283–287 (2000) 1336.